Pathway bias and emergence of quasi-irreversibility in reversible reaction networks: Extension of Curtin-Hammett principle

AUTHOR(S):

Takahashi, Satoshi; Abe, Tsukasa; Sato, Hirofumi; Hiraoka, Shuichi

CITATION:

Takahashi, Satoshi ...[et al]. Pathway bias and emergence of quasi-irreversibility in reversible reaction networks: Extension of Curtin-Hammett principle. Chem 2023, 9(10): 2971-2982

ISSUE DATE:

2023-10-12

URL:

http://hdl.handle.net/2433/285543

Chem

CellPress OPEN ACCESS

Article

Pathway bias and emergence of quasi-irreversibility in reversible reaction networks: Extension of Curtin-Hammett principle

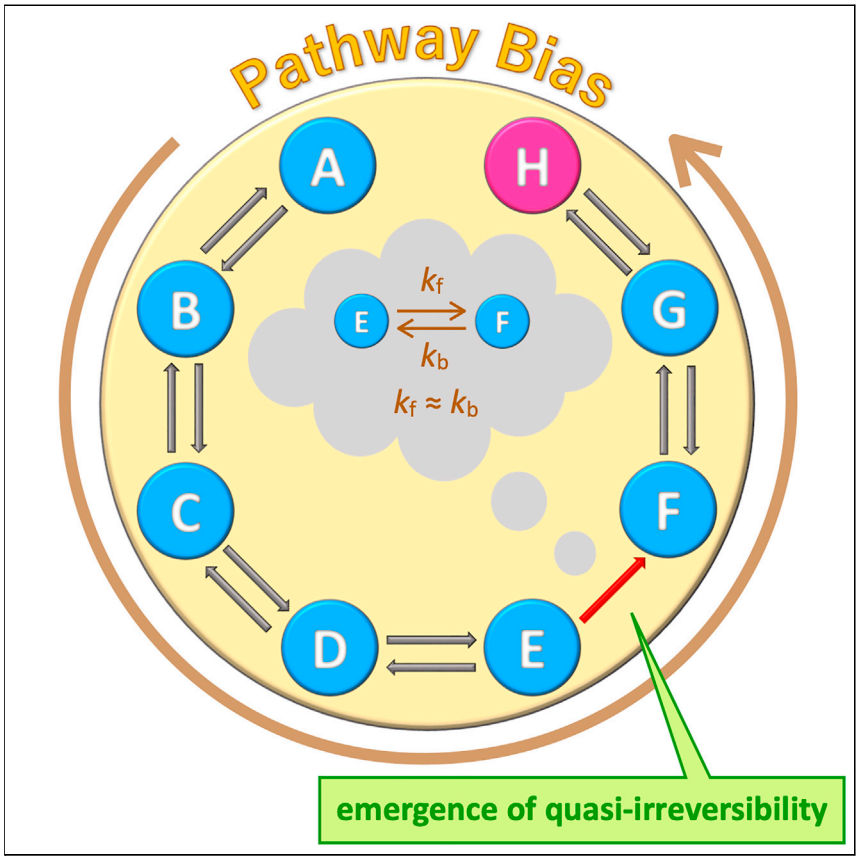

A basic question in reaction networks composed of reversible elementary reactions as seen in protein folding and molecular self-assembly is what the general principle is for the pathway selection. Numerical simulations of model systems and a self-assembly network indicate that the emergence of quasi-irreversibility in certain reaction steps is the key to decision-making, and the selection of quasi-irreversible steps is made as a result of the mutual interactions of the elementary reactions, leading to nonlinear behavior.

Satoshi Takahashi, Tsukasa Abe, Hirofumi Sato, Shuichi Hiraoka

hiraoka-s@g.ecc.u-tokyo.ac.jp

Highlights

Quasi-irreversibility emerges in reaction networks composed of reversible reactions

Transient kinetic state appears even in reversible networks before equilibration

Emergence of quasi-irreversibility is the key to pathway selection in self-assembly

Quasi-irreversible steps in reaction networks are determined in a nonlinear fashion

Takahashi et al., Chem 9, 2971–2982
October 12, 2023
Published by Elsevier Inc.
https://doi.org/10.1016/j.chempr.2023.06.015

Chem

CellPress OPEN ACCESS

Article

Pathway bias and emergence of quasi-irreversibility in reversible reaction networks: Extension of Curtin-Hammett principle

Satoshi Takahashi,[1] Tsukasa Abe,[1] Hirofumi Sato,[2,3] and Shuichi Hiraoka[1,4,*]

SUMMARY

The Curtin-Hammett principle, which works in a reaction sequence where slow irreversible reactions are connected to a fast reversible reaction, determines the product distribution depending only on the relative energy barriers of the two irreversible reactions, resulting in kinetic pathway selection. A basic question is how the reaction pathway is selected in reaction networks composed of reversible reactions to generate a metastable state. Numerical simulations of model systems where reversible elementary reactions are connected linearly to an initial reversible reaction demonstrate that a metastable state far from equilibrium is transiently produced and that its lifetime is prolonged by increasing the number of connected reversible reactions. The pathway selection in the model systems originates from quasi-irreversibility, and a similar behavior was also observed in the molecular self-assembly of a Pd_6L_4 truncated tetrahedron, which supports the idea that the emergence of quasi-irreversibility is a key general concept underlining kinetic control in reversible reaction networks.

INTRODUCTION

Chemical reaction network is the key concept in the origin of functions in living systems, such as regulation,[1–3] amplification,[4,5] oscillation,[6–10] transduction,[11–13] signaling,[14–17] photosynthesis,[18–21] and metabolism.[22–28] Although the kinetics of the elementary reactions in the networks are very simple, unexpected results like emergence are sometimes observed due to mutual correlation among the reactions. Such emergent behaviors have been analyzed and understood by mathematical models,[29–33] which enable us to abstract universality in similar and related phenomena.[34–36] Most of the above-mentioned systems are composed of irreversible reactions, so the direction of each elementary reaction is basically determined. In contrast, it is generally considered that reversible chemical reactions finally reach thermodynamic equilibrium, so the kinetics in reaction networks composed of reversible elementary reactions have been underestimated. Reaction networks composed of reversible elementary reactions are highly adaptive because even the direction of each elementary reaction is affected by other reversible elementary reactions, which is different from irreversible reaction networks. Such reversible reaction networks sometimes lead to metastable, kinetic states as seen in protein folding[37,38] and self-assembly.[39–41] Most of these metastable states are kinetic traps with relatively high kinetic stability and should be selectively produced by pathway selection in the reaction network. However, an understanding of how kinetic traps are produced is elusive because the general principle of pathway selection in reversible reaction networks has not been established yet.

THE BIGGER PICTURE

Finding a general principle through mathematical models enables us to systematically understand natural phenomena and to even make the rational design of novel functions and materials possible based on the principle. A question in this research is what happens at the border between reversibility and irreversibility in chemical reaction networks. Mathematical models demonstrate that the emergence of quasi-irreversibility in certain steps of reversible reaction networks is the key to pathway selection, which even generates a metastable state transiently. This behavior found in reversible networks can be explained by extension of the Curtin-Hammett principle, which will provide a deep insight into the origin of emergent behavior in nature and novel design strategies for the creation of elaborate phenomena in nonlinear systems.

The well-known Curtin-Hammett (C-H) principle[42–46] is a good starting point to consider how the reaction proceeds kinetically in the network containing reversible reaction(s). The simplest reaction network model considered in the C-H principle is shown in Figure 1, where slow irreversible reactions ($A \xrightarrow{k_{AC}} C$ and $B \xrightarrow{k_{BD}} D$) are connected to a fast reversible reaction ($A \rightleftarrows B$). The ratio of the final products (C and D) is not solely determined by the relative proportions of the substrates (A and B), $K_{AB} \equiv k_{AB}/k_{BA}$, yet controlled by the difference in the energy barriers of the two irreversible reactions (k_{AC} and k_{BD}). This indicates that the fate of the reaction is dictated in a kinetically controlled manner. A question arises here: is there a pathway selection principle like the C-H principle for reaction networks composed of only reversible reactions?

Here, we show that quasi-irreversibility appears in reaction networks composed of reversible reactions by numerical simulations of simple mathematical models. It was found that (1) a transient kinetic state is generated even in the network whose elementary reactions are all reversible and that (2) the lifetime of the transient state far from equilibrium is prolonged by increasing the number of connected reversible reactions. Finally, we also found quasi-irreversibility in a complicated reversible network (56 species, 249 elementary reactions), which largely contributes to the pathway selection in the self-assembly of an M_6L_4 coordination cage. The quasi-irreversibility emerged even in reversible elementary reactions with comparable forward and backward rate constants, indicating that mutual interactions among elementary reactions in the network make certain elementary reactions quasi-irreversible. In other words, the reversible reaction network behaves as a nonlinear system, where the function (pathway selection in this case) is not determined by just the sum of properties of each subsystem (rate constants in this case), yet a different property (quasi-irreversibility in this case) emerges due to interactions of the subsystems. Such kinetic-based nonlinear behavior found in a simple artificial system would be helpful to understand primitive evolutional processes and life-like behavior.

RESULTS AND DISCUSSION

Appearance of pathway selection behavior in simple reaction networks consisting of reversible elementary reactions

Starting from the strict C-H system shown in Figure 1, three cases of reaction network models were established (Figure 2). In these models, all the elementary reactions are treated as first-order for simplicity of discussion. In all the numerical simulations the time evolution was traced with the so-called Gillespie algorithm based on the chemical master equation[47–50] (see more detail in the supplemental information; Document S1. Source code is shown in Data S1).

Case 1

In case 1 (Figure 2A), the irreversible $A \xrightarrow{k_{AC}} C$ reaction is as fast as $A \xrightarrow{k_{AB}} B$ in the reversible reaction ($A \rightleftarrows B$), $k_{AC} = k_{AB}$, whereas $k_{AC} < k_{AB}$ in the original C-H model in Figure 1. Although case 1 is no longer the strict C-H condition, it was found that the modification in case 1 makes slight change of the global C-H behavior (Figures 1C and 2A), and less stable C is produced over D in a similar yield of the strict C-H case (blue broken line in Figure 2A). This indicates that the product distribution ([C]/[D]), i.e., the pathway selection, is governed by the rate constants (k_{AC} and k_{BD}) even when the energy barriers between A and B are similar to that of $A \rightarrow C$ ($k_{AC} \simeq k_{AB}$ and k_{BA}). In other words, the irreversibility of the connected reactions ($A \rightarrow C$ and $B \rightarrow D$) is the key to the pathway selection.

Case 2

Next, all the reactions in case 1 are set to be reversible with the rate constants for the backward reactions, $k_{CA} = 10^{-1.5}$ min^{-1} and $k_{DB} = 10^{-2.5}$ min^{-1}, respectively.

[1]Department of Basic Science, Graduate School of Arts and Sciences, the University of Tokyo, 3-8-1 Komaba, Meguro-ku, Tokyo 153-8902, Japan
[2]Department of Molecular Engineering, Kyoto University, Nishikyo-ku, Kyoto 615-8510, Japan
[3]Fukui Institute for Fundamental Chemistry, Kyoto University, Sakyo-ku, Kyoto 606-8103, Japan
[4]Lead contact
*Correspondence: hiraoka-s@g.ecc.u-tokyo.ac.jp
https://doi.org/10.1016/j.chempr.2023.06.015

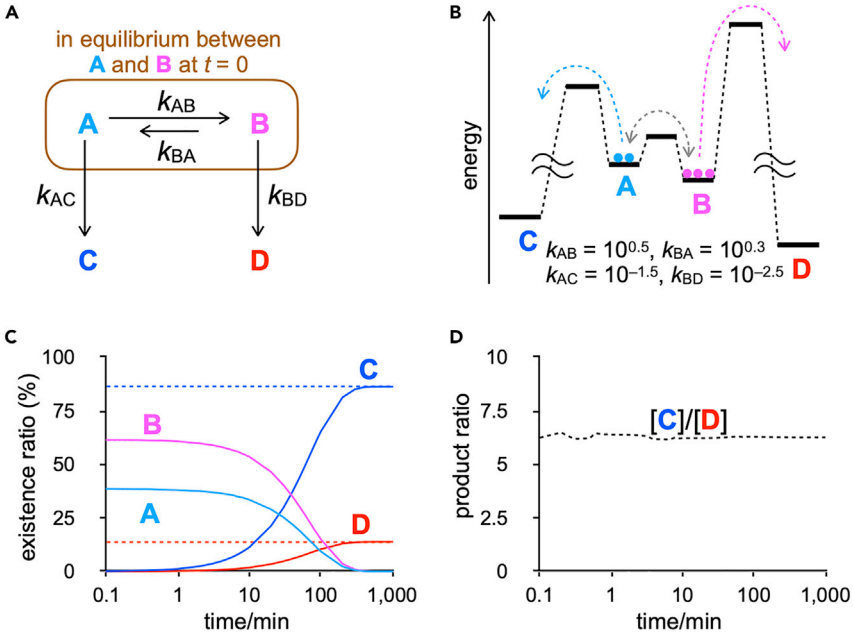

Figure 1. The simplest case of the Curtin-Hammett principle

(A) A reaction network consisting of one reversible reaction (A ⇄ B) with two irreversible reactions (B → D and A → C).

(B) A schematic energy diagram with the corresponding reaction rate constants in the reaction network model shown in (A).

(C) The time evolution of existence ratios of the substrates (A and B) and the products (C and D) obtained by simulation with the initial concentrations given as those at equilibrium between the substrates A and B. Blue and red dashed lines indicate the product ratios in the Curtin-Hammett limit of the global reaction, where the product ratio ([C]/[D]) is calculated to be [C]/[D] = (k_{AC} × k_{BA})/(k_{AB} × k_{BD}) = ($10^{-1.5}$ min^{-1} × $10^{0.3}$ min^{-1})/($10^{0.5}$ min^{-1} × $10^{-2.5}$ min^{-1}) = $10^{0.8}$ = 6.3 (constant).

(D) Time evolution of the product ratio [C]/[D], initially fluctuating a little around and finally reaching 6.3.

Note that for both A ⇄ C and B ⇄ D reactions the backward rate constants are given as 100 times lower than those for the forward ones (Figure 2B). When the system finally reaches the thermodynamic equilibrium, D should be produced more than C because the thermodynamic stability of D is higher than that of C. In numerical simulation, the system reaches the equilibrium state in about 10 h with [D] > [C]. What is interesting is that the situation of [C] > [D] is transiently generated and the ratio of [C]/[D] is similar to that under the C-H condition (cyan-colored region in Figure 2B). This result indicates that the pathway selection like the C-H principle is observed even in a simple reaction network consisting of reversible elementary reactions to generate a transient kinetic state before reaching the global equilibration.

Case 3

Encouraged by the result in case 2, we wonder if the transiently produced kinetic state can be prolonged by connecting reversible reactions in both terminals in case 2 (Figure 2C). Two reversible reactions, C ⇄ E and D ⇄ F, whose rate constants are the same as that of A ⇄ C, are connected to C and D to make a reaction network composed of five reversible reactions. A striking feature found in this reaction network is a significant extension of the transient kinetic state lifetime (for about 1.4 days!).

These results indicate that pathway selection to lead to a metastable, kinetic state is realized even in the reaction network where the elementary reactions are "all

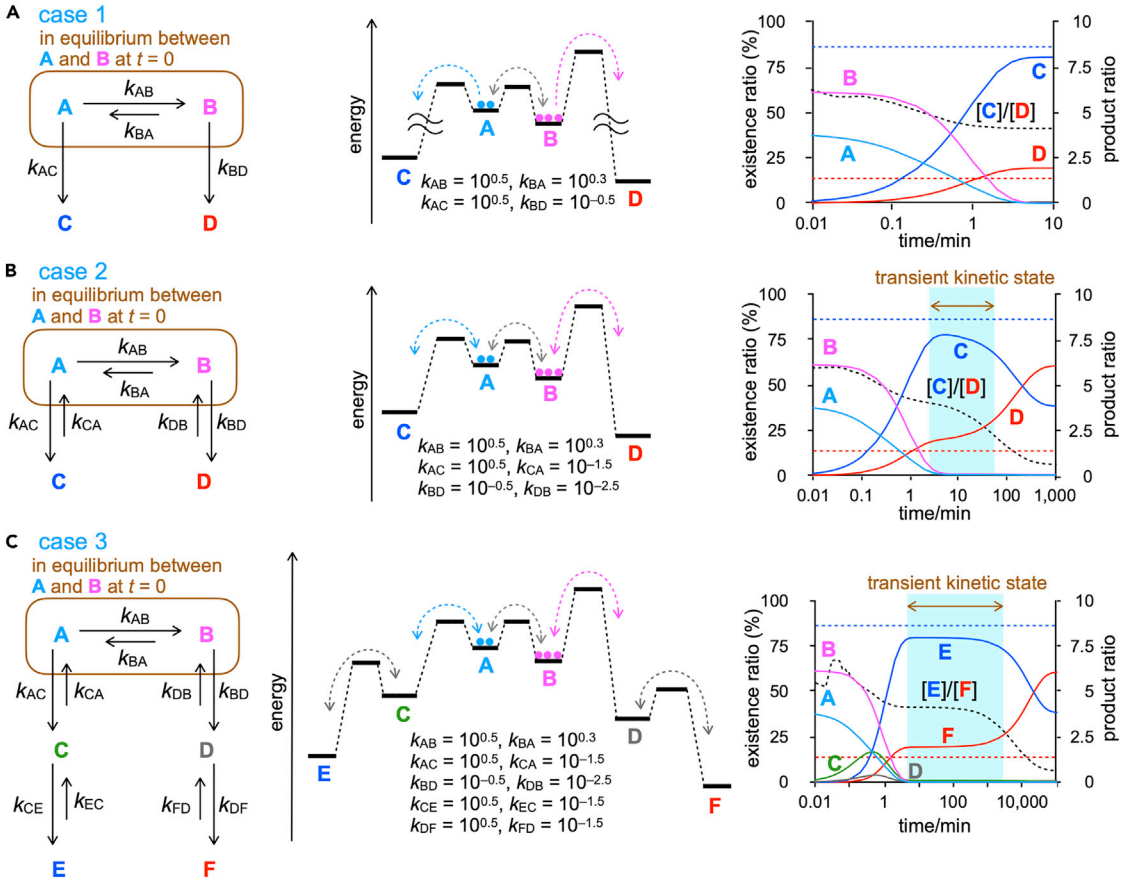

Figure 2. Mathematical models prepared by manipulation of the strict Curtin-Hammett (C-H) situation

(A) The effect of energy barrier of the irreversible **A** → **C** reaction on the product distribution. The difference from the strict C-H system in Figure 1 is that the energy barrier of **A** → **C** is the same as that of **A** → **B** ($k_{AC} = k_{AB}$).

(B) All three elementary reactions are made reversible. A kinetic state is found to hold with a finite lifetime (a cyan rectangle). The product ratio [**C**]/[**D**] in equilibrium is calculated to be [**C**]/[**D**] = ($k_{AC} \times k_{BA} \times k_{DB}$)/($k_{BD} \times k_{AB} \times k_{CA}$) = $10^{(0.5 + 0.3 - 2.5) - (-0.5 + 0.5 - 1.5)}$ = 0.63. The transient kinetic state is indicated by a cyan rectangle.

(C) A reaction network composed of five reversible reactions where two reversible reactions (**C** ⇄ **E** and **D** ⇄ **F**) are connected to **C** and **D** in case 2. Pathway selection to generate a transient kinetic state shown by a cyan rectangle is realized, whose lifetime is prolonged by increasing the number of the reversible reactions, with keeping a product ratio ([**E**]/[**F**]) calculated from the C-H principle. Blue and red broken lines indicate the existence ratios of the final products ([**C**] and [**D**] in case 2, [**E**] and [**F**] in case 3, left vertical axes) in the reaction networks where the elementary reactions except **A** ⇄ **B** are irreversible ($k_{CA} = k_{DB} = k_{EC} = k_{FD} = 0$). Black broken lines indicate the product ratios ([**C**]/[**D**] in case 2, [**E**]/[**F**] in case 3, right vertical axes).

reversible" and that the lifetime of such a transient kinetic state is prolonged by increasing the number of reversible elementary reactions. It should be noted that the transient kinetic state is generated due to the emergence of the quasi-irreversibility of reaction(s) not to high kinetic stability of the metastable state (Figures S1 and S2).

Pathway selection in molecular self-assembly of Pd_6L_4 cage

To see whether the pathway selection is achieved by the emergence of quasi-irreversibility in a more realistic system where many reversible elementary reactions connect with each other like a web, the self-assembly process of a $[Pd_6\mathbf{1}_4]^{12+}$ truncated tetrahedron (TT)[51] was analyzed (Figure 3A). For this system, the possible self-assembly pathways can be classified into the following typical two groups based on the sequence of two kinds of cyclizations, i.e., triangle and square formations (Figure 3B): (path I) square → triangle → triangle, and (path II) triangle → triangle → triangle, so

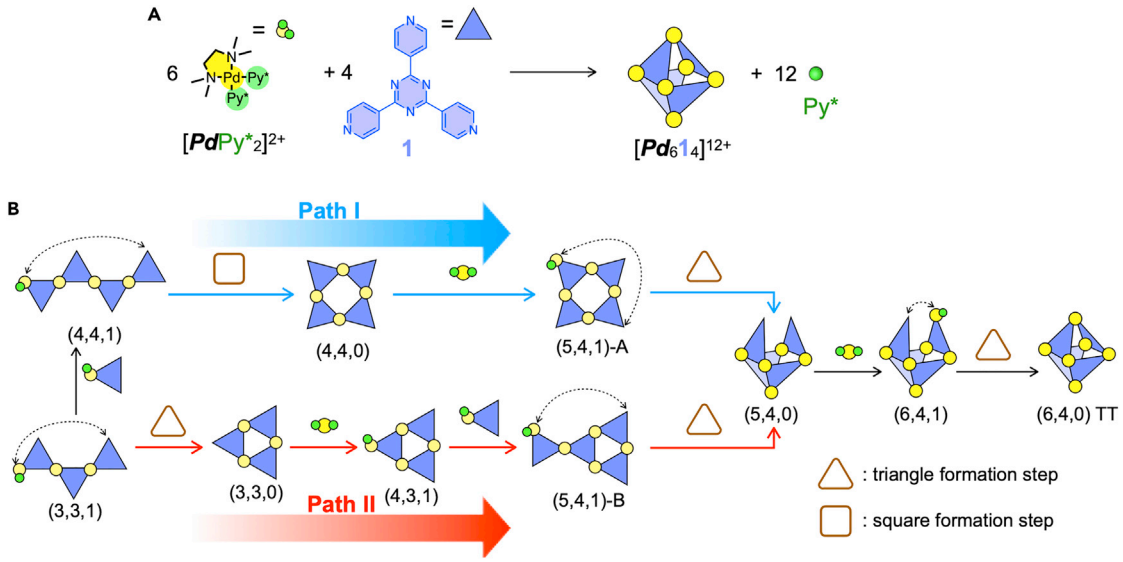

Figure 3. Self-assembly of a $[Pd_6L_4]^{12+}$ truncated tetrahedron (TT) from *cis*-protected Pd(II) complex and tritopic ligand 1

(A) A schematic representation of the self-assembly of a $[Pd_6L_4]^{12+}$ TT. Py* indicates 3-chloropyridine.

(B) Two self-assembly pathways to the $[Pd_6L_4]^{12+}$ TT with a different sequence of three intramolecular steps. Path I with blue arrows indicates a square → triangle → triangle sequence to form the $[Pd_6L_4]^{12+}$ TT, while path II with red arrows indicates that the $[Pd_6L_4]^{12+}$ TT is formed via a triangle → triangle → triangle sequence. (*a*,*b*,*c*) indicates $[Pd_aL_bPy^*_c]^{2a+}$.

the self-assembly of the $[Pd_6L_4]^{12+}$ TT is an appropriate system to discuss the pathway selection, although the final product is the same, unlike the model systems in Figure 2. Considering that the C-H principle is limited to first-order reactions,[43] as most of the elementary reactions in the self-assembly are second-order intermolecular reactions, the self-assembly system deviates from the strict C-H principle.

The self-assembly of the $[Pd_6L_4]^{12+}$ TT was carried out by mixing *cis*-protected Pd(II) complex $[PdPy^*_2]^{2+}$ (*Pd*: Pd(TMEDA), Py*: 3-chloropyridine) and tritopic ligand **1**.[52] The time course of the substrates ($[PdPy^*_2]^{2+}$ and **1**) and the products ($[Pd_6L_4]^{12+}$ and Py*) were monitored by ^{1}H NMR spectroscopy, and the information about the intermediates derived from average composition of all intermediates, *n*-*k* values, were also obtained by quantitative analysis of self-assembly process (QASAP [52–61]) (Figures 4A and 4B. Note that the experimental data are the average of three runs with standard errors). The species in the self-assembly can be generally expressed as $[Pd_aL_bPy^*_c]^{2a+}$, where *a*-*c* indicate the number of components. $[Pd_aL_bPy^*_c]^{2a+}$ is denoted as (*a*,*b*,*c*) for simplicity. Average composition of all intermediates at time *t*, which can be obtained by experiment, is indicated as $[Pd_{\langle a\rangle}L_{\langle b\rangle}Py^*_{\langle c\rangle}]_t$. The intermediates are identified by two parameters, *n* and *k*, which are defined as $n = (2a - c)/b$ and $k = a/b$. The *n* value indicates the average number of *Pd* bound in a single tritopic ligand **1**. The *k* value indicates the ratio of *Pd* against **1**.

The experimental data thus obtained were numerically analyzed by NASAP (numerical analysis of self-assembly process).[52,59–63] A reaction network model composed of 56 species and 249 elementary reactions between them was established (Figure S3), and the search of the rate constants, which are classified into 7 types shown in Figure 4C, in the network giving good fittings of the numerical results to the experimental counterparts was performed (Figures 4A and 4B). The validity of the dataset was confirmed by a good reproduction of the experimental results with different

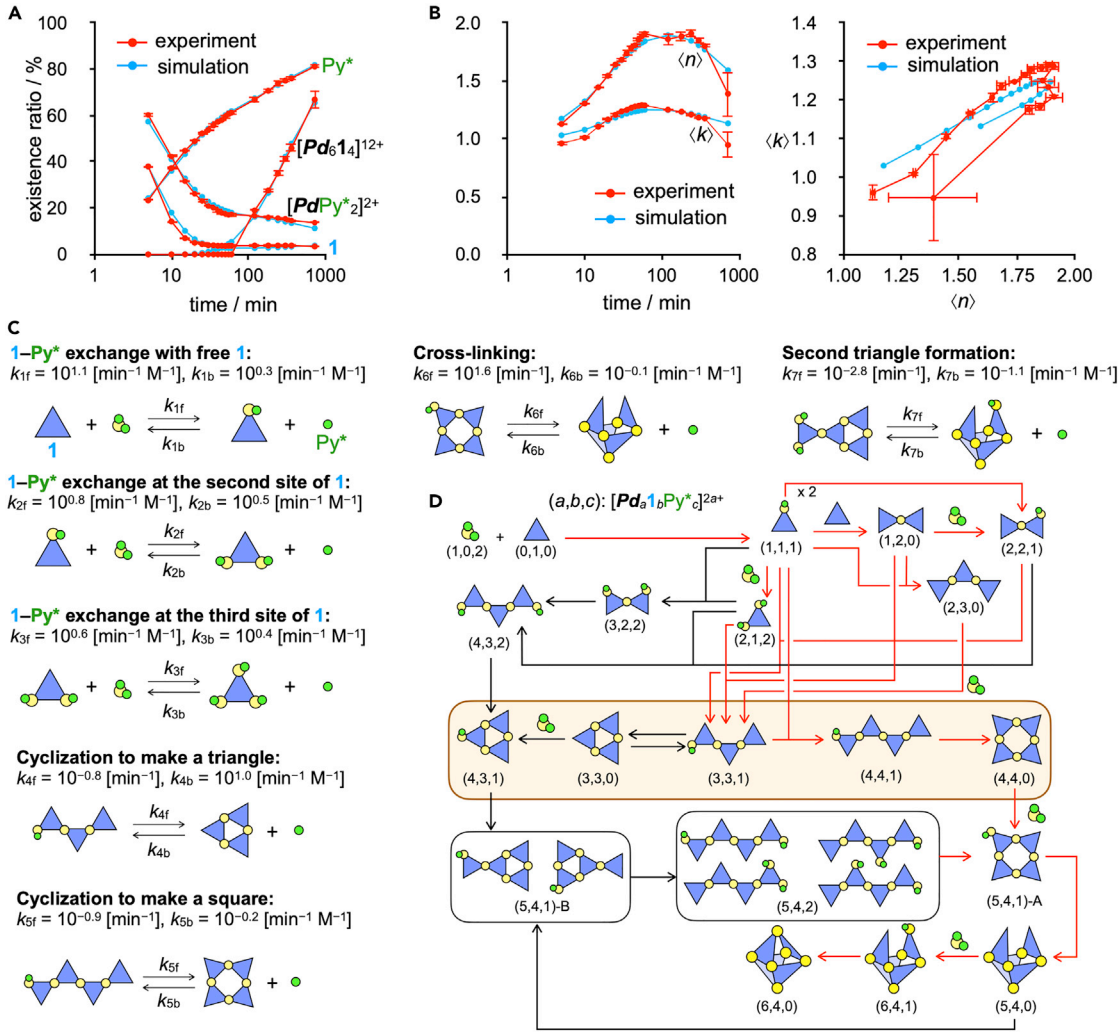

Figure 4. Quantitative analysis of the self-assembly process of the $[Pd_6\mathbf{1}_4]^{12+}$ truncated tetrahedron

(A) Existence ratios of the substrates and products with time. The experimental data are the average of three runs with standard errors.

(B) Changes in the ⟨*n*⟩ and ⟨*k*⟩ values with time. The definition of the *n* and *k* values is indicated in the main text. The experimental data are the average of three runs with standard errors.

(C) 7 types of elementary reactions classified in NASAP and their rate constants determined by numerical fitting to the experimental data in (A) and (B).

(D) Dominant self-assembly pathways determined by numerical simulation with the fixed rate constants. The major self-assembly pathways are indicated by red arrows.

initial stoichiometry of the substrates ($[Pd\mathrm{Py}^*_2]^{2+}$ and **1**, $[Pd]_0/[\mathbf{1}]_0$ = 1.25 and 1.75) (Figures S4 and S5). Base source code for all the simulations is given in Data S2.

With appropriate dataset of the rate constants, we elucidate (1) the main self-assembly pathway and (2) the dominant factors for the pathway selection focusing on the cyclization sequence (path I or II).

Main self-assembly pathway

The main self-assembly pathway in the self-assembly of the $[Pd_6\mathbf{1}_4]^{12+}$ TT, (6,4,0), was determined based on the reaction frequency analysis. The time evolution of the numbers (concentrations) of the species sometimes leads us to an incorrect judgment of the species rapidly converting to the next ones being considered as

intermediates not participating in the major self-assembly pathways. The number of occurrences for each elementary reaction during the focused time region, that is, reaction frequency, is an appropriate parameter to find the major self-assembly pathways.[59] As the elementary reactions in the self-assembly are reversible, the direction of the reaction flow is determined by the difference in frequency between the forward and the backward reactions (we call it the "net reaction frequency"). The main self-assembly pathway(s) can be found by connecting the elementary reactions with the high net reaction frequency (Table S1) from the product (the $[Pd_6\mathbf{1}_4]^{12+}$ TT) to the substrates (**1** and $[Pd\text{Py*}_2]^{2+}$). The main reaction pathway thus obtained (Figure 4D) indicates that the self-assembly of the $[Pd_6\mathbf{1}_4]^{12+}$ TT proceeds mainly through path **I** (square-triangle-triangle sequence).

Emergence of quasi-irreversibility in molecular self-assembly

The pathway selection in the molecular self-assembly can be interpreted by the emergence of quasi-irreversibility. Homology in pathway selection was found between the model reaction networks (Figures 2B and 2C) and the self-assembly of the $[Pd_6\mathbf{1}_4]^{12+}$ TT (Figure 5A). In the model reaction networks, the major pathway is determined by the quasi-irreversibility of **A** ⇄ **C** connected to a reversible reaction (**A** ⇄ **B**). In the self-assembly, a chain of elementary reactions (b), (c), (h), (i), and (j) (a gray area in Figure 5A) corresponds to **A** ⇄ **B** and intermolecular reactions with $[Pd\text{Py*}_2]^{2+}$ (1,0,2), (4,4,0) + (1,0,2) ⇄ (5,4,1)-A + Py* and (5,4,0) + (1,0,2) ⇄ (6,4,1) + Py* ((d) and (f) in Figure 5A), correspond to **A** ⇄ **C** in the model reaction networks.

The reaction rates and the net reaction frequencies of ten elementary reactions (b–k) in Figure 5A are shown in Figures 5B–5K. The most important result is the emergence of quasi-irreversibility in intermolecular reactions in path **I**, (4,4,0) + (1,0,2) $\overset{k_{3f}}{\rightarrow}$ (5,4,1)-A + Py* (Figure 5D) and (5,4,0) + (1,0,2) $\overset{k_{3f}}{\rightarrow}$ (6,4,1) + Py* (Figure 5F), in spite of the rate constant k_{3f} and k_{3b} being comparable ($k_{3f} = 10^{0.6}$, $k_{3b} = 10^{0.4}$ min^{-1} M^{-1}). It should be emphasized that though the same rate constants (k_{3f} and k_{3b}) are given in (3,3,0) + (1,0,2) ⇄ (4,3,1) + Py* in path **II** (Figure 5I) quasi-irreversible behavior was not observed. This contrasting behavior clearly indicates that the self-assembly pathway is not determined solely by the rate constants and that the reaction network structure (mutual interaction among the elementary reactions) is the key factor of pathway selection. The reason why (4,4,0) + (1,0,2) → (5,4,1)-A + Py* (Figure 5D) and (5,4,0) + (1,0,2) → (6,4,1) + Py* (Figure 5F) in path **I** are quasi-irreversible is partly because the products in these steps, (5,4,1)-A and (6,4,1), quickly convert into the next species, (5,4,0) and (6,4,0), by intramolecular bridging reactions, (5,4,1)-A → (5,4,0) + Py* (Figure 5E) and (6,4,1) → (6,4,0) + Py* (Figure 5G). The same analysis of the other elementary reactions in the reaction network of the $[Pd_6\mathbf{1}_4]^{12+}$ TT indicates that quasi-irreversibility appeared in elementary reactions concerning square intermediates (see supplemental information; Data S3).

It is worth discussing why the oligomerization of (3,3,1) to give (4,4,1) followed by the square formation ((4,4,1) → (4,4,0) + Py*, Figure 5C) is preferred to the triangle formation ((3,3,1) → (3,3,0) + Py*, Figure 5H). Considering that generally intramolecular reactions are more advantageous than intermolecular ones at low concentration, under the experimental condition of the self-assembly of the $[Pd_6\mathbf{1}_4]^{12+}$ TT ($[\mathbf{1}]_0$ = 2.0 mM), the triangle formation in path **II**, whose rate constant (k_{4f}) is $10^{-0.8}$ min^{-1}, is expected to take place faster than the oligomerization (path **I**), whose rate constant (k_{2f}) is $10^{0.8}$ min^{-1} M^{-1} ($k_{4f} > k_{2f}\cdot[\mathbf{1}]_0$). As expected, the cyclization of (3,3,1) to form (3,3,0) preferentially occurs until 60 min (a gray line with a red-filled area in Figure 5H). However, the reaction turns in the reverse direction after

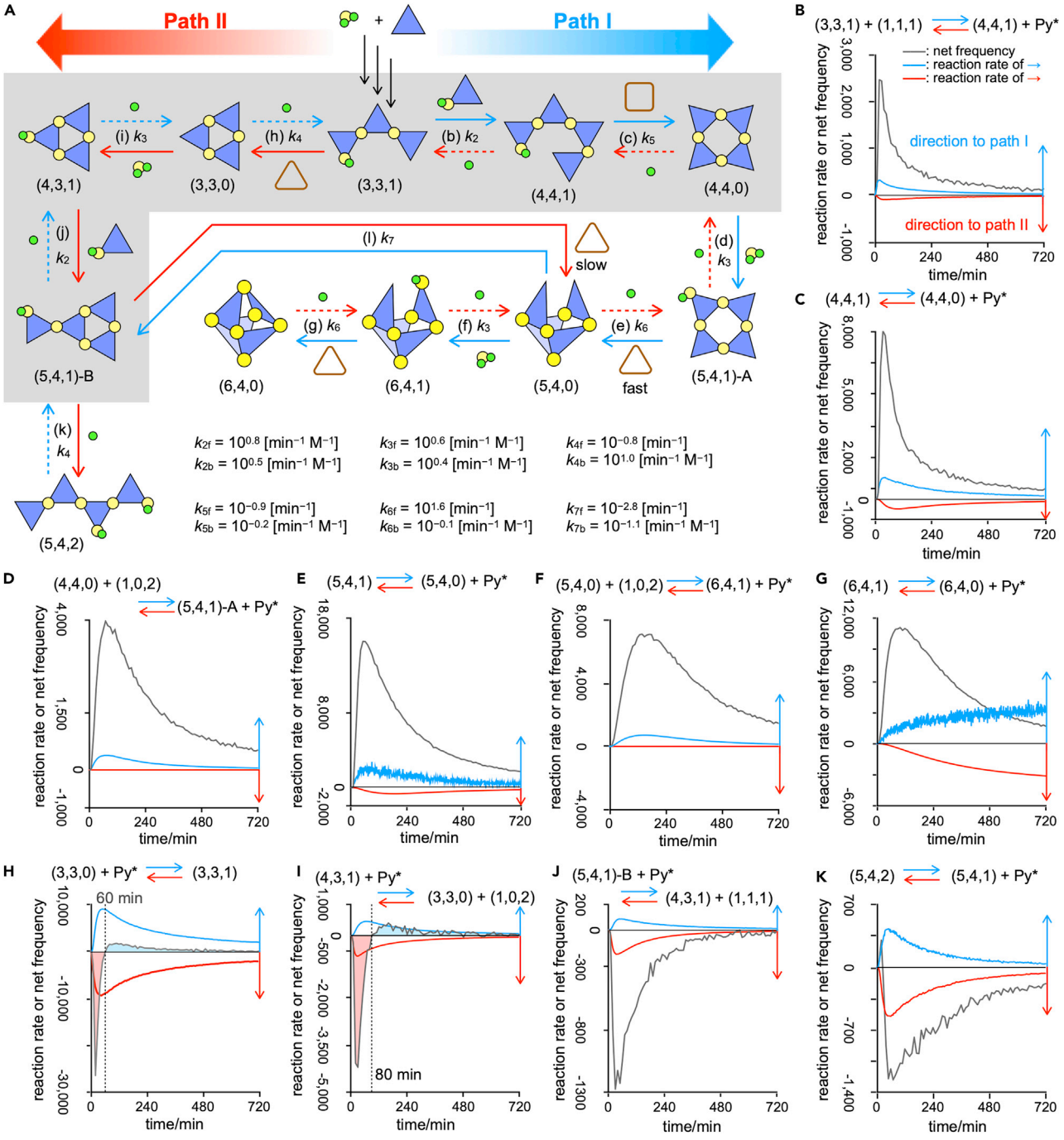

Figure 5. Reaction pathways through triangle and square formations to the $[Pd_6L_4]^{12+}$ truncated tetrahedron

(A) A summary of the pathway selection in the self-assembly by the emergence of quasi-irreversible steps. Reactions in a gray area correspond to a reversible reaction A ⇄ B in the model reaction networks in Figures 2B and 2C, while (4,4,0) + (1,0,2) ⇄ (5,4,1) + Py* and (5,4,0) + (1,0,2) ⇄ (6,4,1) + Py* correspond to quasi-irreversible reaction A ⇄ C.

(B–K) Net frequency and forward and backward reaction rates of the elementary reactions in (A). Alphabetic letters in the reaction arrows in (A) correspond to (B)–(K). Positive values indicate that the reaction proceeds in the blue arrow direction. Switching the direction of the reaction is emphasized by red- and blue-filled areas in (H) and (I). The reaction rate is the quantity defined in the Gillespie algorithm and directly related to the occurrence probabilities for the corresponding elementary reactions. The unit of the reaction rate is (min^{-1} × [number of molecules]) for both the first- (intramolecular) and the second-order (intermolecular) reactions. The time interval for counting the reaction frequency is increased as time proceeds, to avoid the tiny fluctuations counted in shorter time intervals making the reaction directionality get blur.

60 min (a gray line with a blue-filled area in Figure 5H). Similar behavior was found in (3,3,0) + (1,0,2) ⇄ (4,3,1) + Py* in path II (Figure 5I). As to the reactions in path I, the reverse of the reaction direction was not observed, and the forward reactions (blue arrows in Figure 5A) are always dominant (Figures 5B–5G). The switching of the direction of the reactions, (3,3,1) ⇄ (3,3,0) + Py* (Figure 5H) and (3,3,0) + (1,0,2) ⇄ (4,3,1) + Py* (Figure 5I) in path II, is caused by a change in the concentrations of Py* and (3,3,1) during the self-assembly. The concentration of Py* increased with the reaction progress (Figure 4A), and the concentration of (3,3,1) becomes low due to its conversion by the above-mentioned quasi-irreversible steps. Consequently, the oligomerization of (3,3,1) to form (4,4,1) is preferred after 60 min *because of the emergence of quasi-irreversible steps in path I*.

Conclusion

It was found from the numerical analysis that (1) quasi-irreversibility appeared even though the constituent elementary reactions in the network are all reversible, that (2) in a reaction network consisting of many reversible elementary reactions as seen in the self-assembly of the $[Pd_6\mathbf{1}_4]^{12+}$ TT, quasi-irreversibility appeared even in reversible elementary reactions with comparable forward and backward rate constants, and that (3) the quasi-irreversibility in reversible reaction networks is the key to the pathway selection in molecular self-assembly. In self-assembly systems, it is well known that sometimes kinetic traps are obtained because of high energy barriers of their conversion.[37–41,64–66] However, their kinetic stability is not the only reason for their formation, and there should exist the reason why their formation processes are selected. One of the answers to this question is the emergence of quasi-irreversible steps.

From a different perspective, quasi-irreversibility can be said to appear in a nonlinear system in which the constituent elementary reactions interact with each other and exhibit new behavior that cannot be realized by a simple sum of the properties of them. Such a system is never totally reversible and can never be defined as exactly irreversible due to its individual reversible nature. Superlative hybridization of the reversibility and the irreversibility in complicated reaction networks in living systems would be the origin of transient, metastable states that cannot be attained neither in a totally reversible nor in a totally irreversible system.

EXPERIMENTAL PROCEDURES

Resource availability

Lead contact

Further information and requests for resources should be directed to and will be fulfilled by the lead contact, Shuichi Hiraoka (hiraoka-s@g.ecc.u-tokyo.ac.jp).

Materials availability

This study did not generate new materials.

Data and code availability

All the program codes for simulating the reactions on the model networks and searching suitable sets of reaction rate constants are handmade for the purpose of this study. Base source codes are given in supplemental information. Other codes and all the simulation data are available on request from S.T.

SUPPLEMENTAL INFORMATION

Supplemental information can be found online at https://doi.org/10.1016/j.chempr.2023.06.015.

ACKNOWLEDGMENTS

This work was supported by JSPS KAKENHI grant numbers 19H02731, 19K22196, 20K05417, 21K18974, and 23H01970 and the Asahi Glass Foundation. The authors thank Keisuke Takeuchi (the University of Tokyo) for his valuable comments on the manuscript.

AUTHOR CONTRIBUTIONS

S.H. conceived the project. S.T. established mathematical models and carried out all numerical simulation and analysis. T.A. carried out experiments of self-assembly. S.H., S.T., H.S., and T.A. discussed numerical data. S.T. and S.H. prepared the manuscript, and all authors discussed the results and commented on the manuscript.

DECLARATION OF INTERESTS

The authors declare no competing interests.

INCLUSION AND DIVERSITY

We support inclusive, diverse, and equitable conduct of research.

Received: April 4, 2023
Revised: May 12, 2023
Accepted: June 21, 2023
Published: July 18, 2023

REFERENCES

1. Karlebach, G., and Shamir, R. (2008). Modelling and analysis of gene regulatory networks. Nat. Rev. Mol. Cell Biol. *9*, 770–780. https://doi.org/10.1038/nrm2503.

2. Ali Al-Radhawi, M., Del Vecchio, D., and Sontag, E.D. (2019). Multi-modality in gene regulatory networks with slow promoter kinetics. PLoS Comput. Biol. *15*, e1006784. https://doi.org/10.1371/journal.pcbi.1006784.

3. Barbuti, R., Gori, R., Milazzo, P., and Nasti, L. (2020). A survey of gene regulatory networks modelling methods: from differential equations, to Boolean and qualitative bioinspired models. J. Membr. Comput. *2*, 207–226. https://doi.org/10.1007/s41965-020-00046-y.

4. Gerdts, C.J., Sharoyan, D.E., and Ismagilov, R.F. (2004). A synthetic reaction network: chemical amplification using nonequilibrium autocatalytic reactions coupled in time. J. Am. Chem. Soc. *126*, 6327–6331. https://doi.org/10.1021/ja031689l.

5. Kurylo, I., Gines, G., Rondelez, Y., Coffinier, Y., and Vlandas, A. (2018). Spatiotemporal control of DNA-based chemical reaction network via electrochemical activation in microfluidics. Sci. Rep. *8*, 6396. https://doi.org/10.1038/s41598-018-24659-7.

6. Novák, B., and Tyson, J.J. (2008). Design principles of biochemical oscillators. Nat. Rev. Mol. Cell Biol. *9*, 981–991. https://doi.org/10.1038/nrm2530.

7. Li, Z., and Yang, Q. (2018). Systems and synthetic biology approaches in understanding biological oscillators. Quant. Biol. *6*, 1–14. https://doi.org/10.1007/s40484-017-0120-7.

8. Tu, B.P., and McKnight, S.L. (2006). Metabolic cycles as an underlying basis of biological oscillations. Nat. Rev. Mol. Cell Biol. *7*, 696–701. https://doi.org/10.1038/nrm1980.

9. Friesen, W.O., Block, G.D., and Hocker, C.G. (1993). Formal approaches to understanding biological oscillators. Annu. Rev. Physiol. *55*, 661–681. https://doi.org/10.1146/annurev.ph.55.030193.003305.

10. Muñoz, J.J., Dingle, M., and Wenzel, M. (2018). Mechanical oscillations in biological tissues as a result of delayed rest-length changes. Phys. Rev. E *98*, 052409. https://doi.org/10.1103/PhysRevE.98.052409.

11. Helikar, T., Konvalina, J., Heidel, J., and Rogers, J.A. (2008). Emergent decision-making in biological signal transduction networks. Proc. Natl. Acad. Sci. USA *105*, 1913–1918. https://doi.org/10.1073/pnas.0705088105.

12. Bernabò, N., Barboni, B., and Maccarrone, M. (2014). The biological networks in studying cell signal transduction complexity: the examples of sperm capacitation and of endocannabinoid system. Comput. Struct. Biotechnol. J. *11*, 11–21. https://doi.org/10.1016/j.csbj.2014.09.002.

13. Kestler, H.A., Wawra, C., Kracher, B., and Kühl, M. (2008). Network modeling of signal transduction: establishing the global view. BioEssays *30*, 1110–1125. https://doi.org/10.1002/bies.20834.

14. Weng, G., Bhalla, U.S., and Iyengar, R. (1999). Complexity in biological signaling systems. Science *284*, 92–96. https://doi.org/10.1126/science.284.5411.92.

15. Bhalla, U.S. (2003). Understanding complex signaling networks through models and metaphors. Prog. Biophys. Mol. Biol. *81*, 45–65. https://doi.org/10.1016/S0079-6107(02)00046-9.

16. Eungdamrong, N.J., and Iyengar, R. (2004). Modeling cell signaling networks. Biol. Cell *96*, 355–362. https://doi.org/10.1016/j.biolcel.2004.03.004.

17. Otero-Muras, I., Yordanov, P., and Stelling, J. (2017). Chemical reaction network theory elucidates sources of multistability in interferon signaling. PLoS Comput. Biol. *13*, e1005454. https://doi.org/10.1371/journal.pcbi.1005454.

18. Farquhar, G.D., von Caemmerer, S., and Berry, J.A. (1980). A biochemical model of photosynthetic CO_2 assimilation in leaves of C_3 species. Planta *149*, 78–90. https://doi.org/10.1007/BF00386231.

19. Pettersson, G., and Ryde-Pettersson, U. (1988). A mathematical model of the Calvin photosynthesis cycle. Eur. J. Biochem. *175*, 661–672. https://doi.org/10.1111/j.1432-1033.1988.tb14242.x.

20. Nelson, N., and Ben-Shem, A. (2004). The complex architecture of oxygenic photosynthesis. Nat. Rev. Mol. Cell Biol. *5*, 971–982. https://doi.org/10.1038/nrm1525.

21. Stirbet, A., Lazár, D., Guo, Y., and Govindjee, G. (2020). Photosynthesis: basics, history and modelling. Ann. Bot. *126*, 511–537. https://doi.org/10.1093/aob/mcz171.

22. Jahan, N., Maeda, K., Matsuoka, Y., Sugimoto, Y., and Kurata, H. (2016). Development of an accurate kinetic model for the central carbon

metabolism of *Escherichia coli*. Microb. Cell Fact. *15*, 112. https://doi.org/10.1186/s12934-016-0511-x.2.

23. Jeong, H., Tombor, B., Albert, R., Oltvai, Z.N., and Barabási, A.-L. (2000). The large-scale organization of metabolic networks. Nature *407*, 651–654. https://doi.org/10.1038/35036627.

24. Voit, E.O. (2017). The best models of metabolism. Wiley Interdiscip. Rev. Syst. Biol. Med. *9*, e1391. https://doi.org/10.1002/wsbm.1391.

25. Costello, Z., and Martin, H.G. (2018). A machine learning approach to predict metabolic pathway dynamics from time-series multiomics data. npj Syst. Biol. Appl. *4*, 19. https://doi.org/10.1038/s41540-018-0054-3.

26. Shen, F., Sun, R., Yao, J., Li, J., Liu, Q., Price, N.D., Liu, C., and Wang, Z. (2019). OptRAM: in-silico strain design via integrative regulatory-metabolic network modeling. PLoS Comput. Biol. *15*, e1006835. https://doi.org/10.1371/journal.pcbi.1006835.

27. Kurata, H. (2021). Virtual metabolic human dynamic model for pathological analysis and therapy design for diabetes. iScience *24*, 102101. https://doi.org/10.1016/j.isci.2021.102101.

28. Uematsu, S., Ohno, S., Tanaka, K.Y., Hatano, A., Kokaji, T., Ito, Y., Kubota, H., Hironaka, K.I., Suzuki, Y., Matsumoto, M., et al. (2022). Multi-omics-based label-free metabolic flux inference reveals obesity-associated dysregulatory mechanisms in liver glucose metabolism. iScience. iScience *25*, 103787. https://doi.org/10.1016/j.isci.2022.103787.

29. Feinberg, M. (1987). Chemical reaction network structure and the stability of complex isothermal reactors—I. The deficiency zero and deficiency one theorems. Chem. Eng. Sci. *42*, 2229–2268. https://doi.org/10.1016/0009-2509(87)80099-4.

30. Feinberg, M. (1988). Chemical reaction network structure and the stability of complex isothermal reactors—II. Multiple steady states for networks of deficiency one. Chem. Eng. Sci. *43*, 1–25. https://doi.org/10.1016/0009-2509(88)87122-7.

31. Robinson, W.E., Daines, E., van Duppen, P., de Jong, T., and Huck, W.T.S. (2022). Environmental conditions drive self-organization of reaction pathways in a prebiotic reaction network. Nat. Chem. *14*, 623–631. https://doi.org/10.1038/s41557-022-00956-7.

32. Huang, S., Li, F., Zhou, J.X., and Qian, H. (2017). Processes on the emergent landscapes of biochemical reaction networks and heterogeneous cell population dynamics: differentiation in living matters. J. R. Soc. Interface *14*, 20170097. https://doi.org/10.1098/rsif.2017.0097.

33. van Roekel, H.W.H., Rosier, B.J.H.M., Meijer, L.H.H., Hilbers, P.A.J., Markvoort, A.J., Huck, W.T.S., and de Greef, T.F.A. (2015). Programmable chemical reaction networks: emulating regulatory functions in living cells using a bottom-up approach. Chem. Soc. Rev. *44*, 7465–7483. https://doi.org/10.1039/C5CS00361J.

34. Barzel, B., and Barabási, A.L. (2013). Universality in network dynamics. Nat. Phys. *9*, 673–681. https://doi.org/10.1038/nphys2741.

35. Fiedler, B., Mochizuki, A., Kurosawa, G., and Saito, D. (2013). Dynamics and control at feedback vertex sets. I: Informative and determining nodes in regulatory networks. J. Dyn. Diff. Equat. *25*, 563–604. https://doi.org/10.1007/s10884-013-9312-7.

36. Mochizuki, A., Fiedler, B., Kurosawa, G., and Saito, D. (2013). Dynamics and control at feedback vertex sets. II: a faithful monitor to determine the diversity of molecular activities in regulatory networks. J. Theor. Biol. *335*, 130–146. https://doi.org/10.1016/j.jtbi.2013.06.009.

37. Varela, A.E., England, K.A., and Cavagnero, S. (2019). Kinetic trapping in protein folding. Protein Eng. Des. Sel. *32*, 103–108. https://doi.org/10.1093/protein/gzz018.

38. Mecha, M.F., Hutchinson, R.B., Lee, J.H., and Cavagnero, S. (2022). Protein folding in vitro and in the cell: from a solitary journey to a team effort. Biophys. Chem. *287*, 106821. https://doi.org/10.1016/j.bpc.2022.106821.

39. Suzuki, A., Aratsu, K., Datta, S., Shimizu, N., Takagi, H., Haruki, R., Adachi, S.I., Hollamby, M., Silly, F., and Yagai, S. (2019). Topological impact on the kinetic stability of supramolecular polymers. J. Am. Chem. Soc. *141*, 13196–13202. https://doi.org/10.1021/jacs.9b06029.

40. Yoneya, M., Tsuzuki, S., Yamaguchi, T., Sato, S., and Fujita, M. (2014). Coordination-directed self-assembly of $M_{12}L_{24}$ nanocage: effects of kinetic trapping on the assembly process. ACS Nano *8*, 1290–1296. https://doi.org/10.1021/nn404595j.

41. Hagan, M.F., Elrad, O.M., and Jack, R.L. (2011). Mechanisms of kinetic trapping in self-assembly and phase transformation. J. Chem. Phys. *135*, 104115. https://doi.org/10.1063/1.3635775.

42. Gold, V. (1979). Glossary of terms used in physical organic chemistry. Pure Appl. Chem. *51*, 1725–1801. https://doi.org/10.1351/pac197951081725.

43. Seeman, J.I., Sanders, E.B., and Farone, W.A. (1980). Uses and analyses of Curtin-Hammett/Winstein-Holness systems involving second order reactions. Tetrahedron *36*, 1173–1177. https://doi.org/10.1016/0040-4020(80)87014-1.

44. Seeman, J.I. (1983). Effect of conformational change on reactivity in organic chemistry. Evaluations, applications, and extensions of Curtin-Hammett Winstein-Holness kinetics. Chem. Rev. *83*, 83–134. https://doi.org/10.1021/cr00054a001.

45. Seeman, J.I. (1986). The Curtin-Hammett principle and the Winstein-Holness equation: new definition and recent extensions to classical concepts. J. Chem. Educ. *63*, 42. https://doi.org/10.1021/ed063p42.

46. Chakraborty, S., and Saha, C. (2016). The Curtin-Hammett principle. Resonance *21*, 151–171. https://doi.org/10.1007/s12045-016-0307-7.

47. Gillespie, D.T. (1976). A general method for numerically simulating the stochastic time evolution of coupled chemical reactions. J. Comput. Phys. *22*, 403–434. https://doi.org/10.1016/0021-9991(76)90041-3.

48. Gillespie, D.T. (1977). Exact stochastic simulation of coupled chemical reactions. J. Phys. Chem. *81*, 2340–2361. https://doi.org/10.1021/j100540a008.

49. Gillespie, D.T. (1992). A rigorous derivation of the chemical master equation. Phys. Stat. Mech. Appl. *188*, 404–425. https://doi.org/10.1016/0378-4371(92)90283-V.

50. Gillespie, D.T. (2007). Stochastic simulation of chemical kinetics. Annu. Rev. Phys. Chem. *58*, 35–55. https://doi.org/10.1146/annurev.physchem.58.032806.104637.

51. Fujita, M., Oguro, D., Miyazawa, M., Oka, H., Yamaguchi, K., and Ogura, K. (1995). Self-assembly of ten molecules into nanometre-sized organic host frameworks. Nature *378*, 469–471. https://doi.org/10.1038/378469a0.

52. Komine, S., Takahashi, S., Kojima, T., Sato, H., and Hiraoka, S. (2019). Self-assembly processes of octahedron-shaped Pd_6L_4 cages. J. Am. Chem. Soc. *141*, 3178–3186. https://doi.org/10.1021/jacs.8b12890.

53. Baba, A., Kojima, T., and Hiraoka, S. (2015). Self-assembly process of dodecanuclear Pt(II)-linked cyclic hexagon. J. Am. Chem. Soc. *137*, 7664–7667. https://doi.org/10.1021/jacs.5b04852.

54. Tsujimoto, Y., Kojima, T., and Hiraoka, S. (2014). Rate-determining step in the self-assembly process of supramolecular coordination capsules. Chem. Sci. *5*, 4167–4172. https://doi.org/10.1039/C4SC01652A.

55. Kai, S., Sakuma, Y., Mashiko, T., Kojima, T., Tachikawa, M., and Hiraoka, S. (2017). The effect of solvent and coordination environment of metal source on the self-assembly pathway of a Pd(II)-mediated coordination capsule. Inorg. Chem. *56*, 12652–12663. https://doi.org/10.1021/acs.inorgchem.7b02152.

56. Hiraoka, S. (2015). What do we learn from the molecular self-assembly process? Chem. Rec. *15*, 1144–1147. https://doi.org/10.1002/tcr.201510005.

57. Hiraoka, S. (2018). Unresolved issues that remain in molecular self-assembly. Bull. Chem. Soc. Jpn. *91*, 957–978. https://doi.org/10.1246/bcsj.20180008.

58. Hiraoka, S. (2019). Self-assembly processes of Pd(II)- and Pt(II)-linked discrete self-assemblies revealed by QASAP. Isr. J. Chem. *59*, 151–165. https://doi.org/10.1002/ijch.201800073.

59. Takahashi, S., Tateishi, T., Sasaki, Y., Sato, H., and Hiraoka, S. (2020). Towards kinetic control of coordination self-assembly: a case study of a Pd_3L_6 double-walled triangle to predict the outcomes by a reaction network model. Phys. Chem. Chem. Phys. *22*, 26614–26626. https://doi.org/10.1039/d0cp04623j.

60. Zhang, X., Takahashi, S., Aratsu, K., Kikuchi, I., Sato, H., and Hiraoka, S. (2022). Cyclization or bridging: which occurs faster is the key to the self-assembly mechanism of Pd_6L_3coordination prisms. Phys. Chem. Chem.

Phys. *24*, 2997–3006. https://doi.org/10.1039/D1CP04448F.

61. Hiraoka, S., Takahashi, S., and Sato, H. (2021). Coordination self-assembly processes revealed by collaboration of experiment and theory: toward kinetic control of molecular self-assembly. Chem. Rec. *21*, 443–459. https://doi.org/10.1002/tcr.202000124.

62. Matsumura, Y., Hiraoka, S., and Sato, H. (2017). A reaction model on the self-assembly process of octahedron-shaped coordination capsules. Phys. Chem. Chem. Phys. *19*, 20338–20342. https://doi.org/10.1039/c7cp03493h.

63. Takahashi, S., Sasaki, Y., Hiraoka, S., and Sato, H. (2019). A stochastic model study on the self-assembly process of a Pd_2L_4 cage consisting of rigid ditopic ligands. Phys. Chem. Chem. Phys. *21*, 6341–6347. https://doi.org/10.1039/C8CP06102E.

64. Shin, S.-H., Chung, S., Sanii, B., Comolli, L.R., Bertozzi, C.R., and De Yoreo, J.J. (2012). Direct observation of kinetic traps associated with structural transformations leading to multiple pathways of S-layer assembly. Proc. Natl. Acad. Sci. USA *109*, 12968–12973. https://doi.org/10.1073/pnas.1201504109.

65. Treiber, D.K., and Williamson, J.R. (1999). Exposing the kinetic traps in RNA folding. Curr. Opin. Struct. Biol. *9*, 339–345. https://doi.org/10.1016/S0959-440X(99)80045-1.

66. Yan, Y., Huang, J., and Tang, B.Z. (2016). Kinetic trapping - strategy for directing the self-assembly of unique functional nanostructures. Chem. Commun. (Camb) *52*, 11870–11884. https://doi.org/10.1039/C6CC03620A.